IJARST

International Journal of Advanced Research in Science and Technology

https://doi.org/10.62226/ijarst20262707

ISSN 2319 – 1783 (Print)

ISSN 2320 – 1126 (Online)

Biogenic Synthesis of AgO Nanoparticles Using *Thunbergia erecta* Leaf Extract: Characterization and Enhanced H_2S Gas Sensing Performance

Sonali. P. Nikam[1], Sachin. S. Kushare*[2], Ujjan. B. Kadam*[1]

[1]Research Centre, Department of Chemistry, MGV. M.S.G.Arts, Science, and Commerce College, Malegaon. (MH), India-423105

[2]Research Centre, Department of Chemistry, MVP Samaj's K.K.Wagh Arts, Science and Commerce College Pimpalgaon (B)(MH), India-422009

Corresponding author Email Id- sachinkushare7@gmail.com, kadumub64@gmail.com

ARTICLEINFO

Article history:

Received	12 June 2026
Accepted	27 June 2026
Available online	30 June 2026

Keywords:

AgO nanoparticles; Green synthesis; Thunbergia erecta; Biogenic synthesis; Gas sensor; H_2S detection; Sensitivity; Low operating temperature.

Indexed in:

and in major libraries

ABSTRACT

The current study used Thunbergia erecta leaf extract as a reducing and stabilising agent to biogenically synthesise silver oxide (AgO) nanoparticles in an economical and environmentally friendly manner. X-ray diffraction (XRD), scanning electron microscopy (SEM), transmission electron microscopy (TEM), energy-dispersive X-ray spectroscopy (EDX), and Fourier transform infrared spectroscopy (FTIR) were used to systematically characterise the synthesised nanoparticles in order to verify their crystalline nature, morphology, elemental composition, and surface functional groups. The creation of well-crystalline, quasi-spherical AgO nanoparticles with uniform distribution and nanoscale dimensions was demonstrated by the results. The produced AgO nanoparticles' ability to detect different gases, such as H_2S, CO, CO_2, NH_3 and H_2, was examined. Among these, the sensor showed outstanding selectivity and sensitivity in reaction to hydrogen sulphide (H_2S). The sensor reached a maximum sensitivity of 120.21 toward H_2S gas at a particular concentration at the ideal operating temperature of 100 °C. The high surface-to-volume ratio, enhanced adsorption capacity, and the presence of active surface sites made possible by phytochemical residues from the plant extract are all responsible for the improved sensing performance. The produced AgO nanoparticles are a potential option for effective H_2S gas detection in industrial safety and environmental monitoring applications due to their superior sensing properties, low working temperature, and green manufacturing method.

1. Introduction

Material science has developed as an encouraging topic of nanoscience due to its considerable applications in research. Adsorption, photocatalysis, biosensors, solar cells, conducting material, drug distribution, photovoltaic, pharmaceutical, agricultural, and catalytical applications, photoreduction, sultriness sensors [1-3], and sensors [4,5] are all considered. Massive pollution and industrial dangers are currently the major threats to the environment. The creation of dangerous substances and emissions from transportation and industry are the main sources of pollutant gases. These hazardous gases that are harmful to the environment must be recognised so that the threats caused by gas leakage and gas emission can be identified as soon as possible. Gas sensors are often a straightforward material used to identify minute gas quantities at different places [6]. Since the catalyst is crucial to the sensitivity of semiconducting ceramic gas sensors, it has been thoroughly studied. For gas detection, hetero connections between p- and n-type semiconducting grains have been developed recently [7-10]. These semiconducting gas sensors are able to identify traces of dangerous substances in the air, which sets them apart from single oxide semiconductors. The search for new, high-quality gas-sensing materials as well as unique characteristics of already-existing materials has grown in importance. CuO-SnO_2 [16,17], WO_3 [11-13], and CuO-doped SnO_2 [14]-based thin-film or thick-film sensors have shown exceptional performance in the detection of diluted H_2S less than 1 ppm.

Recently, nano phased WO_3-based H_2S gas sensors for ppb-level H_2S detection have been reported [15]. Exposure of humans to H_2S gas at concentrations more than 250 parts per million is likely to cause neurobehavioral harm and may even be fatal [16]. Over the past few decades, a wide range of industries, including environmental analysis, the automotive sector, medical applications, and indoor air quality controls, have developed and employed novel gas sensors [17-20].Monitoring dangerous gases including CO, CO_2, NOx (x=0.5, 1, and 2), SOx (x=2 and 3), and NH_3 is becoming more and more important as concerns about the

environment and human health grow. Ammonia (NH_3) gas detection has drawn a lot of attention in the field of gas sensors among these hazardous gas species. This is important since NH_3 is one of the most widely produced and used compounds in many different parts of the world [21-25]. Approximately 80% of NH_3 was created recently for nitrogen-based fertiliser, with the remaining 20% going toward refrigeration, pharmaceuticals, cleaning products, and explosives. Fruit and vegetable juice, petrochemical facilities, dairy and ice cream plants, wineries and breweries, and soft drink manufacturing industries are common locations for NH_3 [26,27].

Additionally, NH_3 is widely used in cars, especially diesel engines, to reduce hazardous NOx emissions by selective catalytic reduction (SCR) because it is a good source of hydrogen [28,29]. The Occupational Safety and Health Administration (OSHA) states that the maximum amount of NH_3 that humans can be exposed to is 25 parts per million (ppm) for eight hours and 35 parts per million (ppm) for ten minutes [30]. Furthermore, NH_3 is categorised as an environmental contaminant because it is very reactive and reacts with nitric acid and sulphuric acid in the air to form aerosols like ammonium nitrate and ammonium sulphate. These nanosized NH_3 particles consequently create smog, which has a cooling effect and negatively affects the global greenhouse balance [31-34]. Additionally, monitoring NH_3 with breath analysers is an essential daily clinical practice routine for patients with lung or renal disorders, since exhaled NH_3 in human breath is one of the critical markers for identifying those conditions [35]. By enabling the manipulation of materials at the nanoscale, where novel physical, chemical, and biological properties develop, nanotechnology has revolutionised modern science and technology. Because of their high surface-to-volume ratio, tunable optical characteristics, and high reactivity, metal and metal oxide nanoparticles in particular have drawn a lot of attention. These characteristics make them appropriate for a variety of applications, such as environmental remediation, biomedical engineering, sensing, and catalysis [36].

Because of their remarkable antibacterial activity, catalytic efficiency, optical properties, and chemical stability, silver-based nanomaterials in particular, silver oxide (AgO) nanoparticles have been thoroughly investigated [37]. AgO nanoparticles are highly desirable for application in drug delivery systems, gas sensing technologies, antibacterial coatings, and wastewater treatment because of their characteristics. Historically, physical and chemical techniques such sol-gel processes, hydrothermal synthesis, chemical reduction, and precipitation have been used to create silver oxide nanoparticles [38]. These methods often involve hazardous chemicals, require a lot of energy, and have complicated processing conditions, even if they provide controlled particle size and form. Due to the formation of hazardous byproducts, these limitations not only increase manufacturing costs but also seriously impair the environment and human health [39].

In this study, the selectivity of various gases was evaluated after the gas sensing property of thick films was examined for a number of gases, including CO_2, CO, H_2, NH_3, and H_2S, at different operating temperatures while keeping a constant gas concentration. The produced nanocrystalline materials were characterised using FTIR, XRD, SEM, TEM, and BET. As a crucial meterological element, the AgO nanoparticle sensor with varying amounts of H_2S gas was also investigated.

2. Experimental

2.1 Materials

Starting components included precursor silver nitrate $AgNO_3$ and sodium hydroxide (NaOH). To make leaf extract, fresh leaves of the blue flower plant, Thunbergia erecta, were gathered. Every chemical utilised was analytical grade and didn't require any additional purification. The experiment was conducted using distilled water.

2.2 Preparation of *Thunbergia erecta* Leaf Extract

To get rid of dust and contaminants, fresh Thunbergia erecta leaves were carefully cleaned with distilled water. After cleaning, the leaves were coarsely chopped and cooked for 15 to 20 minutes in distilled water. Whatman filter paper was used to filter the extract once it had cooled to room temperature. The filtrate was kept in storage and utilised as a stabilising and reducing agent.

2.3 Synthesis of AgO Nanoparticles

To synthesise AgO nanoparticles, an aqueous solution of silver nitrate (0.01 M) was produced. The Thunbergia erecta leaf extract was added dropwise to the $AgNO_3$ solution with steady magnetic stirring at room temperature. A considerable colour change suggested the reduction of Ag^+ ions. To create silver oxide nanoparticles, add a few drops of NaOH solution to alter the pH to alkaline (pH ~ 10-12). To guarantee that all nanoparticles were formed, the reaction mixture was agitated constantly for 2-3 hours. The precipitate was separated by centrifugation at 5000-8000 rpm for 10-15 minutes, then washed multiple times with distilled water and ethanol to eliminate contaminants. The filtered product was then dried in a hot air furnace at 80-100 °C for many hours. Finally, the dried sample was calcined in a muffle furnace at 400-600°C for 4-6 hours to produce crystalline AgO nanoparticles.

2.4 Characterization

The AgO nanoparticles products were characterised using analytical methods. Using a Shimadzu 8400S FTIR spectrophotometer, (KBr pellets) were analysed using Fourier-transform infrared spectroscopy (FT-IR) in the 4000–400 cm^{-1} range. The phase purity of the product was determined using an X-ray powder diffraction pattern utilising Rigaku Ultima IV copper equipment operating at 25 kV and 25 mA using CuK radiation with a wavelength of 0.154 nm and Bragg's scanning angle varying from 10º to 80º. Using a scanning electron microscope (FESEM) (FEI Nova Nano SEM 450 equipment, with an elemental resolution of 0.14 nm), the material's surface morphology and properties were verified. The crystallinity, morphological features, and crystal type of AgO nanoparticles were determined. The Quantachrome Autosorb Automated Gas Sorption System Autosorb-1, NOVA-1200, and Mercury Porosimeter

Autosorb-1c were used to evaluate the BET surface area using the N_2 adsorption desorption isotherm.

3. Results and Discussion

3.1. Functional group analysis using FT-IR spectroscopy

To determine the functional groups on the surface of the produced AgO nanoparticles and to comprehend the function of phytochemicals (if green synthesis is applied) in reduction and stabilisation, FTIR spectroscopy was utilised shows in Fig.1. AgO nanoparticles' FTIR spectra usually exhibit a number of distinctive absorption bands that correspond to surface functional groups and metal oxygen interaction. The creation of silver oxide nanoparticles is confirmed by a prominent absorption band in the 480 cm^{-1} range, which is attributable to the Ag–O stretching vibration. This band is a crucial sign that the AgO synthesis was effective. O–H stretching vibrations are shown by broad absorption peaks about 3200–3500 cm^{-1}, which could be caused by hydroxyl groups on the surface of the nanoparticle or adsorbed water molecules. This band also shows the presence of phenolic compounds from plant extracts that serve as capping and reducing agents in green synthesis processes. The peaks at 1500–1400 cm^{-1} are typically attributed to H-O-H bending vibrations or C=O stretching (amide I), indicating the presence of proteins or biomolecules that could stabilise the nanoparticles. Similarly, symmetric stretching of carboxylate groups or C–H bending vibrations are linked to bands around 1400–1450 cm^{-1}. The C–O stretching vibrations of alcohols, esters, or ethers are responsible for absorption peaks in the 1000–1300 cm^{-1} range, suggesting the role of organic molecules in the stabilisation of nanoparticles. Furthermore, ambient CO_2 adsorption may be the cause of faint peaks at 2300 cm^{-1}. The existence of these functional groups demonstrates that biomolecules, including proteins, terpenoids, and flavonoids, are adsorbed on the surface of AgO nanoparticles and are essential to their synthesis and stabilisation. These functional groups improve the physicochemical characteristics of the nanoparticles while also preventing agglomeration.

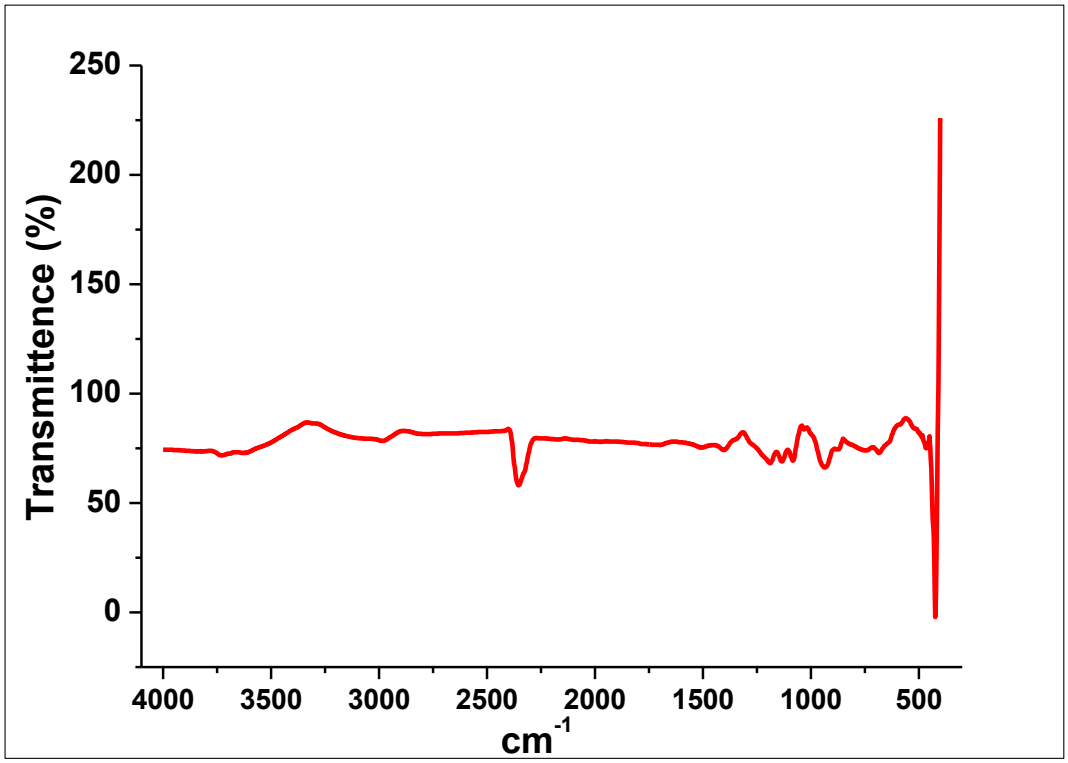

Fig. 1. FT-IR spectra of AgO nanoparticles

3.2. X-ray Diffraction (XRD) Analysis of AgO Nanoparticles

X-ray diffraction (XRD) analysis was used to assess the crystalline structure and phase purity of the produced silver oxide nanoparticles (Fig.2.). Cu Kα radiation (λ = 1.5406 Å) was used to capture the diffraction pattern in the 2θ range, which is normally 20°-80°. The production of monoclinic AgO (silver(II) oxide) was confirmed by indexing and comparing the observed diffraction peaks with standard data from the ICDD Powder Diffraction File (PDF No. 84-1108). The crystallographic planes (111), (200), (220), (311), and (222) are represented by the conspicuous diffraction peaks seen at around 2θ = 32.3°, 38.1°, 55.0°, 65.7°, and 69.2°, respectively. These reflections show successful synthesis because they agree well with the typical AgO phase. Indicating that the produced nanoparticles had a high phase purity. A high level of crystallinity is indicated by the peaks' sharpness and intensity.

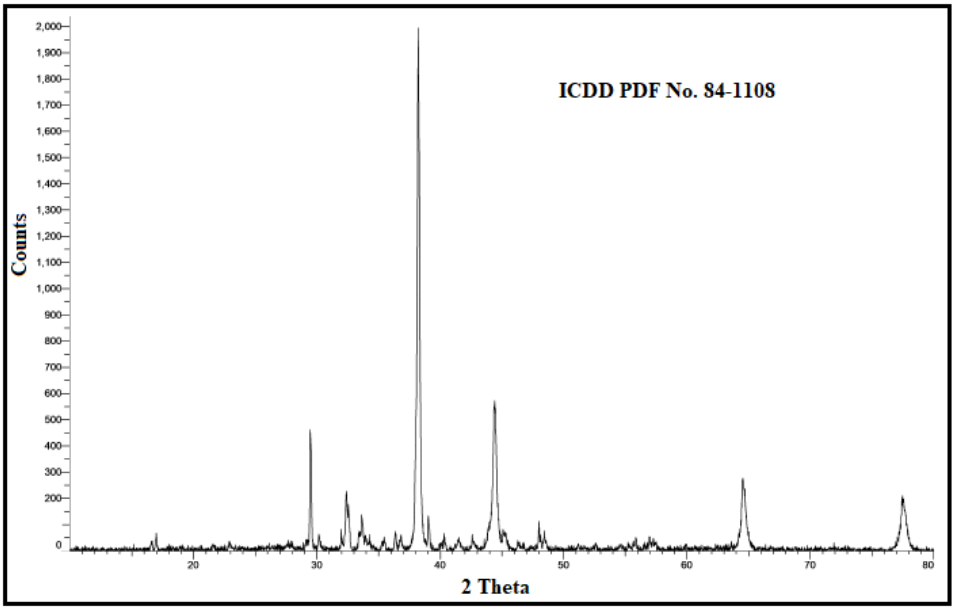

Fig. 2. XRD pattern of AgO Nanoparticles

3.3. Scanning Electron Microscopy (SEM) Analysis of AgO Nanoparticles

Scanning electron microscopy (SEM) was used to examine the surface morphology and microstructural characteristics of the produced silver oxide (AgO) nanoparticles. The produced AgO nanoparticles have a non-uniform, aggregated shape, which is typical of metal oxide nanoparticles because of their high surface energy, according to the SEM images. The particles show up as dense clusters at reduced magnification, suggesting a propensity for agglomeration. Strong interparticle interactions like van der Waals forces during the synthesis and drying processes are responsible for this aggregation. The individual particles are shown to have rough surfaces and irregular to spherical forms at greater magnifications. The estimated particle size from SEM pictures is consistent with nanoscale dimensions, ranging from about 20-80 nm (or adjust based on your data). The aggregation of smaller crystallites into larger particles is probably the reason why the observed particle size is marginally larger than the crystallite size determined by XRD analysis. The nanoparticles' uneven and porous surface may increase their surface reactivity and make them appropriate for uses like sensing, catalysis, and antibacterial activity. The synthesis process successfully created nanosized AgO particles, as evidenced by the lack of significant bulk structures

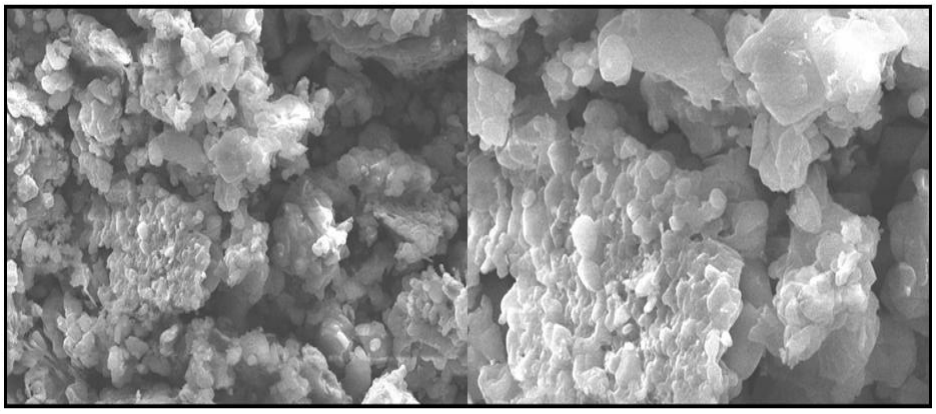

Fig.3. Scanning Electron Microscopy (SEM) Images of AgO nanoparticles

3.4. Energy Dispersive X-ray (EDX) Analysis of AgO Nanoparticles

To investigate the spatial distribution of elements in the produced AgO nanoparticles, elemental mapping analysis was performed using an EDS connected to a SEM. The homogenous generation of silver oxide is confirmed by the mapping images, which clearly demonstrate Fig.4(a). the uniform distribution of oxygen (O) and silver (Ag) throughout the sample. Ag (Lα emission) is responsible for the strong and distinct peaks at about ~3.1 keV, whereas O (Kα emission) is responsible for the peak at around ~0.5 keV. Because silver has a greater atomic number and a higher X-ray emission efficiency than oxygen, the high intensity of the silver peak is expected. The O mapping likewise displays a well-dispersed signal, suggesting that oxygen is uniformly connected with silver in the nanoparticle structure, whereas the Ag mapping image Fig.4(b) displays a strong and consistent intensity throughout the whole region. The effective production of AgO without phase separation is further supported by the overlap of Ag and O signals. The mapping images showed no discernible signals of

other elements, indicating the great purity and lack of contaminants in the produced nanoparticles. The consistent elemental distribution indicates that the chosen synthesis technique is successful in creating AgO nanostructures that are compositionally homogeneous.

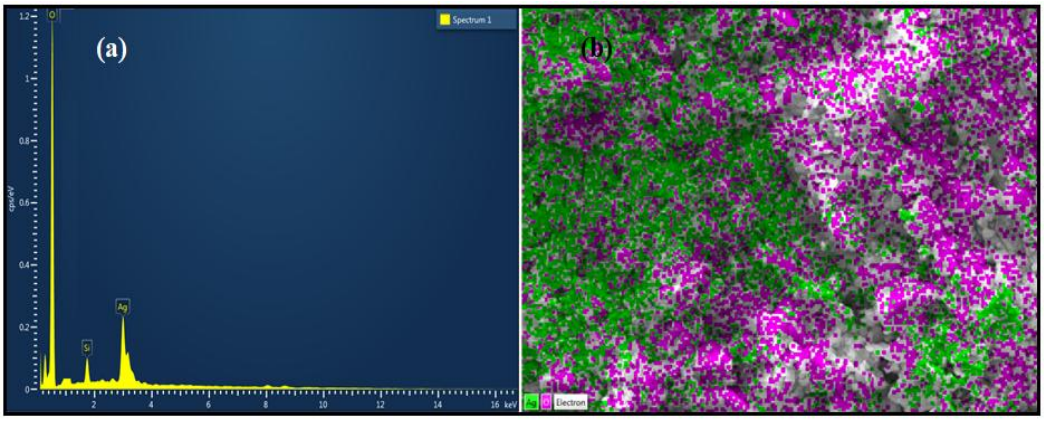

Fig.4(a). Energy Dispersive X-ray (EDX) and Fig.4(b) Mapping image of AgO nanoparticles

3.5. Transmission Electron Microscopy (TEM) and SAED Analysis of AgO Nanoparticles

Transmission electron microscopy (TEM) was used to further analyse the size, shape, and internal structure of the produced silver oxide (AgO) nanoparticles (Fig.5a). The TEM photos show that the AgO nanoparticles are primarily spherical or irregular in shape, depending on your image, and have a propensity to form small agglomerations. This is common for nanoscale metal oxides because of their high surface energy. The crystallite size determined from XRD data closely matches the particle size observed from TEM examination, which ranges between ~10–40 nm (replace with your actual range). A regulated synthesis process is shown by the comparatively narrow size distribution. Certain areas exhibit distinct particle boundaries, indicating well-defined nanostructures. If used, high-resolution TEM (HRTEM) confirms the crystalline structure of the nanoparticles by displaying clear lattice fringes. Phase identification is further supported by the measured interplanar spacing (d-spacing), which correlates well with the typical planes of monoclinic AgO (e.g., ~0.24 nm or according to your data). The Selected Area Electron Diffraction (SAED) (Fig.5b) pattern further verified the AgO nanoparticles' crystallinity. Instead of distinct spots, the SAED image shows a sequence of concentric diffraction rings, which indicates that the sample is polycrystalline. In accordance with the standard ICDD PDF data of AgO (PDF No. 84-1108), the rings were indexed to particular lattice planes such (111), (200), (220), and (311) (check with your data). Good crystallinity of the nanoparticles is indicated by the vivid and distinct diffraction rings. The effective synthesis of nanocrystalline AgO with great structural integrity is confirmed by the agreement between SAED, TEM, and XRD data.

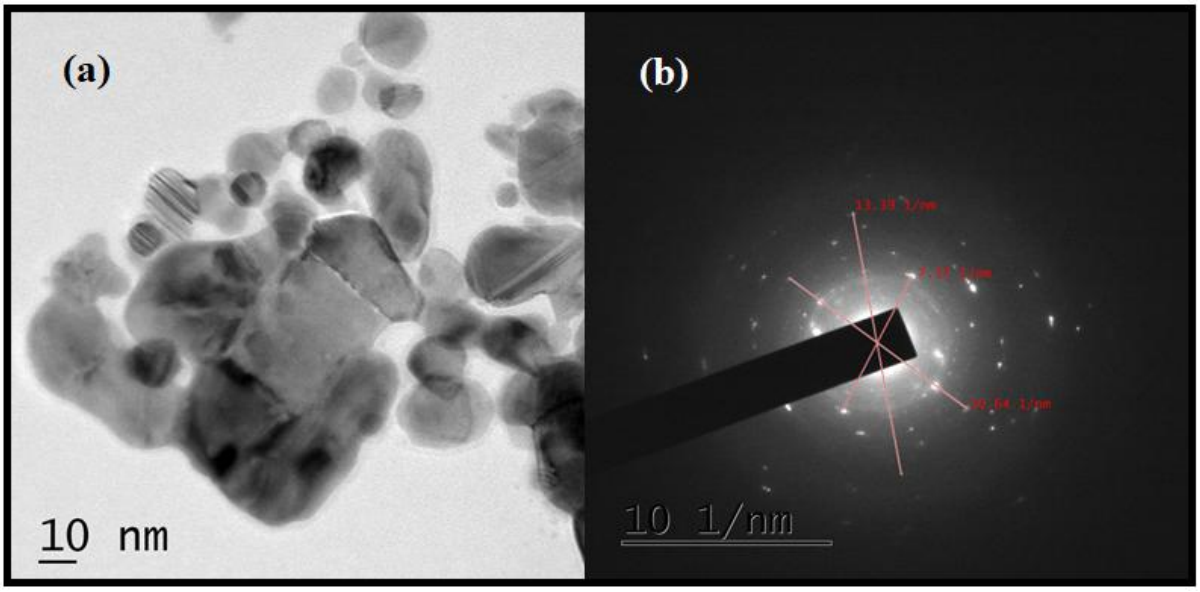

Fig.5(a) Transmission Electron Microscopy and Fig.5(b) SAED Image of AgO nanoparticles

4. Response of AgO Nanoparticles for the Selected Gases

According to the literature, the sensor operating temperature affects the surface adsorption/desorption processes and the change in the energy required to activate them, making sensitivity, selectivity, and response time temperature-dependent factors. Figure 6 illustrates how different gases affect

AgO nanoparticles in relation to temperature. Feeding temperature in the presence of a particular gas can be used to determine a sensor's sensitivity and selectivity. Conclusions regarding a material's gas detecting capability and the cost of constructing a gas monitoring sensor can be made once the selectivity and sensitivity have been calculated. The characteristics of gas detection are strongly influenced by the kind of adsorption on the sensor surface. Depending on the type of adsorption, gas sensing adsorption in metal oxide base semiconducting materials may differ. based on the information gathered regarding the gases' selectivity. The selectivity of sensing materials, such as silver oxide, towards different gases, such as CO, CO_2, NH_3, H_2, and H_2S, is shown in Figure 5. The operating temperature variation from 50 to 400°C with 100 ppm of each gas is also depicted in Figure 6. According to the results, the thick sheet of AgO nanoparticles provides greatest sensitivity for H_2S gas (120.21) at 100 °C, NH_3 (95.11) at 100 °C, and H_2 (88.20) at 150 °C. It is the best option for H_2S gas and a very uncommon occurrence, according to the data gathered from the selectivity of the gases. AgO nanoparticles showed a number of intriguing characteristics.

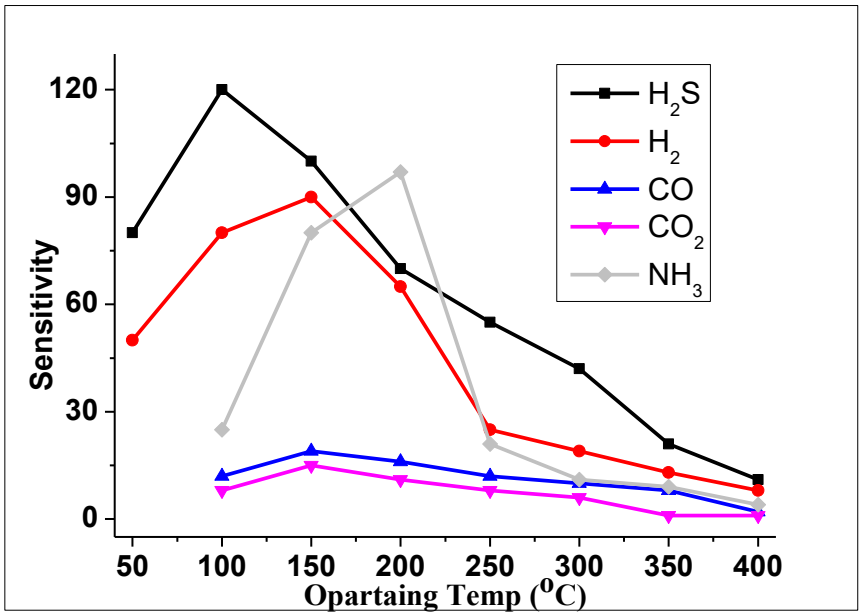

Fig.6.Sensitivity verses operating temperature for AgO Nanoparticles

4.1 Effect of Operating Temperature AgO Nanoparticles for H2S Gas

The sensing properties of synthesised AgO nanomaterials thick films were investigated in this study by conducting experiments against various operation temperatures (50-400 ºC). According to the current study, the sensitivity of AgO nanoparticles is affected by annealing temperatures between 100 and 400 ºC, as shown in Fig. 7. Under the same annealing temperature conditions, H_2S gas (100 ppm) gas for AgO thick films at different temperatures was also investigated. To determine its structure and achieve crystallisation, the sensing material is annealed at different temperatures. Because achieving the appropriate electrical properties which are crucial for gas sensor applications requires a certain degree of crystallinity. Figure 5 shows that the AgO thick film with an annealing temperature of 400 ºC had the highest sensitivity at an operating temperature of 100 ºC. The gas response grows as the operating temperature rises, reaching its maximum at 400 ºC, thanks to the thick sheets and sensors made for every sample. The catalytic capabilities of metal nanoparticles are often diminished at high operating temperatures (>400 °C) because they tend to aggregate in larger-sized clusters, which reduces their surface area and, thus, their gas sensitivity.

In order to return resistance to the initial baseline with a complete recovery without losing the catalytic actions of metal nanoparticles, light heating at 150–250 °C promotes the desorption of the gaseous species from the surface of the sensing active layer. It was found that annealing in air promotes the production of oxygen vacancies, which raises the amount of H_2S gas-sensing AgO nanoparticles. Additionally, careful monitoring reveals that the sensitivity rises between 350 and 400 °C.

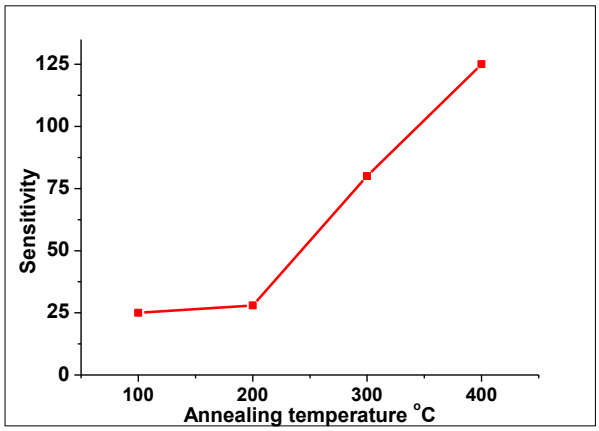

Fig.7. Sensitivity verses annealing temperature at operating temperature of H_2S gas for AgO nanoparticles

4.2 Effect of Concentration of H_2S Gas

The sensitivity to H_2S gas concentrations (20–120 ppm) at a thick film annealing temperature of 400 ºC is shown in Figure 8. It has been noted that prepared sensors exhibit a significant increase in sensitivity. In this investigation, the exposure of 100 ppm of H_2S gas to AgO at an operating temperature of 100 ºC produced the greatest response. As the gas concentration increased, the sensors' sensitivity to the gas was found to be improved, most likely as a result of additional gas molecules building up on their surface. The response of gases is caused by the adsorption of reacting gaseous molecules on the sensor surface. According to the current investigation, AgO showed the greatest response when exposed to 100 ppmof H2S gas at an operating temperature of 100 ºC.

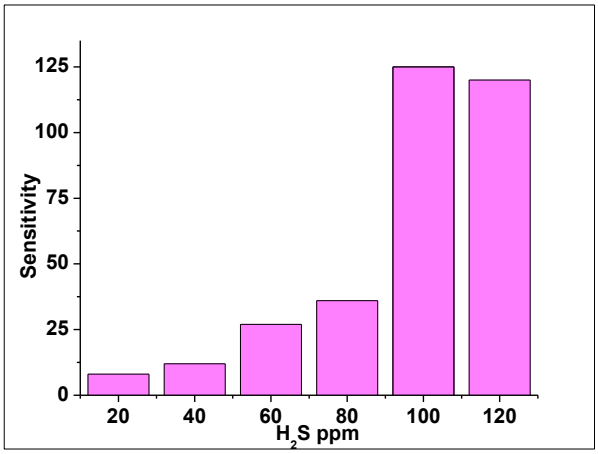

Fig.8. Variation of response with H_2S gas concentration for AgO nanoparticles

5. Conclusions

In this study, AgO nanoparticles were effectively synthesised using Thunbergia erecta leaf extract in an environmentally friendly and sustainable way. Structural, morphological, and compositional analyses confirmed the production of well-crystalline nanoparticles with uniform distribution and nanoscale dimensions. The phytochemical-assisted synthesis enhanced surface activity and provided an environmentally safe pathway. The gas sensing capabilities of the generated AgO nanoparticles demonstrated a strong and targeted response to H2S gas. The sensor showed an optimal operating temperature of 100 °C with a maximum sensitivity of 120.21. Furthermore, between 100-400 °C, the effect of annealing temperature on sensing performance was carefully investigated. The results showed that the sample that was annealed at 400 °C exhibited superior sensing properties, which may be related to higher crystallinity and charge transport. Additionally, the effect of gas concentration was evaluated throughout the 20–120 ppm range. The highest response the sensor displayed at 100 ppm of H_2S revealed its exceptional detection capability within this concentration range. The primary reasons for the improved sensing behaviour are the increased adsorption–desorption kinetics and the availability of active sites on the nanoparticle surface. Overall, because of their green manufacture, optimal annealing temperature, and excellent sensing performance at low operating temperatures, the generated AgO nanoparticles are a promising material for practical H_2S gas sensing applications in industrial safety and environmental monitoring.

References

[1] B. Baruwati, K. M. Reddy, S. V. Manorama, R. K. Singh, O. Parkash, "Tailored conductivity behavior in nanocrystalline nickel ferrite," *Applied Physics Letters*, vol. 85, no. 14, pp. 2833–2835, 2004. https://doi.org/10.1063/1.1801685

[2] J. Guo, H. Jia, A. Zhang, Z. Pei, M. Luo, J. Xue, Q. Shen, X. Liu, B. Xu, "MIL-100 (Fe) with mix-valence coordinatively unsaturated metal site as Fenton-like catalyst for efficiently removing tetracycline hydrochloride: Boosting Fe(III)/Fe(II) cycle by photoreduction," *Separation and Purification Technology*, vol. 262, p. 118334, 2021. https://doi.org/10.1016/j.seppur.2021.118334

[3] A. V. Borhade, D. R. Tope, J. A. Agashe, S. S. Kushare, "Synthesis, Characterization and Photocatalytic study of FeCr2O4@ZnO@MgO Core-Shell Nanoparticle," *Journal of Water and Environmental Nanotechnology*, vol. 6, no. 2, pp. 164-176, 2021. https://doi.org/10.22090/JWENT.2021.02.006

[4] A. V. Borhade, D. R. Tope, S. S. Kushare, S. V. Thakare, "Fly ash supported NiO as an efficient catalyst for the synthesis of xanthene and its molecular docking study against plasmodium glutathione reductase," *Research on Chemical Intermediates*, vol. 44, no. 12, pp. 7459-7478, 2018. doi.org

[5] S. S. Kushare, V. D. Bobade, V. N. Suryawanshi, D. R. Tope, A. V. Borhade, "Synthesis and Characterization of Novel CoCr2O4@GeO2@ZnO Core–Shell Nanostructure: Focus on Electrical Conductivity and Gas Sensing Properties," *Journal of Inorganic and Organometallic Polymers and Materials*, vol. 32, no. 7, pp. 2679-2693, 2022. https://doi.org/10.1007/s10904-022-02309-w

[6] A. V. Borhade, V. D. Bobade, DR Tope, J. A. Agashe, S. S. Kushare, "A Highly Selective and Sensitive H2S Gas Sensor Based on Novel Nanostructure Core–Shell FeCr2O4@ZnO@MgO," *Journal of Inorganic and Organometallic Polymers and Materials*, vol. 31, no. 12, pp. 4670-4683, 2021. https://doi.org/10.1007/s10904-021-02072-4

[7] J. Shan, P. Bougiatioti, L. Liang, G. Reiss, T. Kuschel, B. J. van Wees, "Nonlocal magnon spin transport in NiFe2O4 thin films," *Applied Physics Letters*, vol. 110, no. 13, p. 132406, 2017. https://doi.org/10.1063/1.4979408

[8] E. Traversa, M. Miyayama, H. Yanagida, "Gas sensitivity of ZnO/La2CuO4 hetero-contacts,"

Sensors and Actuators B: Chemical, vol. 17, no. 3, pp. 257-261, 1994. https://doi.org/10.1016/0925-4005(94)87020-7

[9] J. Tamaki, T. Maekawa, N. Miura, N. Yamazoe, "Sensing behaviour of CuO-loaded SnO2 element for H2S detection," *Sensors and Actuators B: Chemical*, vol. 9, no. 3, pp. 197-203, 1992. https://doi.org/10.1016/0925-4005(92)80216-K

[10] J. Tamaki, K. Shimanoe, Y. Yamada, Y. Yamamoto, N. Miura, N. Yamazoe, "Gas-sensing properties of SnO2 thin films fabricated by laser ablation," *Sensors and Actuators B: Chemical*, vol. 49, no. 1-2, pp. 121–125, 1998. https://doi.org/10.1016/S0925-4005(98)00044-5

[11] D. J. Yoo, J. Tamaki, S. J. Park, N. Miura, N. Yamazoe, "Copper Oxide-Loaded Tin Dioxide Thin Film for Detection of Dilute Hydrogen Sulfide," *Japanese Journal of Applied Physics*, vol. 34, no. 4A, pp. L455–L457, 1995. https://doi.org/10.1143/JJAP.34.L455

[12] J. L. Solis, S. Saukko, L. B. Kish, C. G. Granqvist, V. Lantto, "Nanocrystalline tungsten oxide thick-films with high sensitivity to H2S at room temperature," *Sensors and Actuators B: Chemical*, vol. 77, no. 1-2, pp. 316-321, 2001. https://doi.org/10.1016/S0925-4005(01)00735-6

[13] J. L. Solis, S. Saukko, L. B. Kish, C. G. Granqvist, V. Lantto, "Semiconductor gas sensors based on nanostructured tungsten oxide," *Thin Solid Films*, vol. 391, no. 2, pp. 255–260, 2001. https://doi.org/10.1016/S0040-6090(01)00953-7

[14] J. L. Solis, A. Hoel, L. B. Kish, C. G. Granqvist, S. Saukko, V. Lantto, "Conduction Properties of Nanocrystalline WO3 Films Made by Advanced Reactive Gas Deposition," *Journal of the American Ceramic Society*, vol. 84, no. 7, pp. 1504-1508, 2001. https://doi.org/10.1111/j.1151-2916.2001.tb00873.x

[15] R. Kumar, A. Khanna, P. Tripathi, R. V. Nandedkar, S. R. Potdar, S. M. Chaudhari, S. S. Bhatti, "Effect of substrate temperature on structural, optical and electrical properties of reactive dc magnetron sputtered tungsten oxide thin films," *Journal of Applied Physics*, vol. 93, no. 4, pp. 2377–2381, 2003. https://doi.org/10.1063/1.1542655

[16] R. Ionescu, A. Hoel, C. G. Granqvist, E. Llobet, P. Heszler, "Low-power consumption gas sensor for toxic gas detection based on nanostructured WO3," *Sensors and Actuators B: Chemical*, vol. 104, no. 1, pp. 132-139, 2005. https://doi.org/10.1016/j.snb.2004.04.030

[17] N. Tamaekong, C. Liewhiran, A. Wisitsoraat, S. Phanichphant, "Sensing Characteristics of Flame-Spray-Pyrolyzed WO3 Nanoparticles for H2S Detection," *Sensors*, vol. 10, no. 8, pp. 7863-7873, 2010. https://doi.org/10.3390/s100807863

[18] S. J. Kim, I. S. Hwang, Y. C. Kang, J. H. Lee, "Highly Sensitive and Selective H2S Sensors Using Pt-Loaded WO3 Heptagonal Nanorings," *Sensors*, vol. 11, no. 11, pp. 10603-10614, 2011. https://doi.org/10.3390/s111110603

[19] I. C. Chen, S. S. Lin, T. J. Lin, C. L. Hsu, T. J. Hsueh, T. Y. Shieh, "Gas Sensing Properties of Hexagonal WO3 Nanorods Synthesized by a Hydrothermal Process," *Sensors*, vol. 10, no. 4, pp. 3057-3072, 2010. https://doi.org/10.3390/s100403057

[20] A. Fuerte, R. X. Valenzuela, M. J. Escudero, L. Daza, "Ammonia chemisorption and reactivity on tungsten oxide powders," *Journal of Power Sources*, vol. 192, no. 1, pp. 170-174, 2009. https://doi.org/10.1016/j.jpowsour.2008.12.093

[21] L. Zhang, W. Yang, "High-temperature ammonia sensor based on tungsten oxide thick film," *Journal of Power Sources*, vol. 179, no. 1, pp. 92-95, 2008. https://doi.org/10.1016/j.jpowsour.2008.01.028

[22] A. Chellappa, C. Fischer, W. Thomson, "Ammonia decomposition kinetics over tungsten oxide catalysts," *Applied Catalysis A: General*, vol. 227, no. 1-2, pp. 231-240, 2002. https://doi.org/10.1016/S0926-860X(01)00967-3

[23] T. Hejze, J. O. Besenhard, K. Kordesch, M. Cifrain, R. R. Aronsson, "Tungsten oxides as alternative anode materials for lithium-ion batteries," *Journal of Power Sources*, vol. 176, no. 2, pp. 490-493, 2008. https://doi.org/10.1016/j.jpowsour.2007.08.070

[24] M. Comotti, S. Frigo, "Hydrogen generation system based on ammonia decomposition for fuel cell vehicles," *International Journal of Hydrogen Energy*, vol. 40, no. 33, pp. 10673-10686, 2015. https://doi.org/10.1016/j.ijhydene.2015.06.113

[25] R. Lan, J. T. S. Irvine, S. Tao, "Ammonia and related chemicals as potential indirect hydrogen storage materials," *International Journal of Hydrogen Energy*, vol. 37, no. 2, pp. 1482-1494, 2012. https://doi.org/10.1016/j.ijhydene.2011.09.048

[26] G. K. Mani, J. B. B. Rayappan, "A highly sensitive and selective room temperature ammonia gas sensor based on spray pyrolyzed ZnO thin film," *Applied Surface Science*, vol. 311, pp. 405-412, 2014. https://doi.org/10.1016/j.apsusc.2014.05.066

[27] S. Giddey, S. P. S. Badwal, A. Kulkarni, "Review of electrochemical ammonia production technologies and materials," *International Journal of Hydrogen Energy*, vol. 38, no. 34, pp. 14576-14594, 2013. https://doi.org/10.1016/j.ijhydene.2013.09.054

[28] B. Timmer, W. Olthuis, A. Van Den Berg, "Ammonia sensors and their applications—a review," *Sensors and Actuators B: Chemical*, vol.

107, no. 2, pp. 666-677, 2005. https://doi.org/10.1016/j.snb.2004.11.054

[29] G. K. Mani, J. B. B. Rayappan, "Influence of Al doping on the structural, optical and ammonia sensing properties of ZnO thin films," *Materials Science and Engineering: B*, vol. 191, pp. 41-50, 2015. doi.org

[30] G. K. Mani, J. B. B. Rayappan, "Highly sensitive room temperature ammonia sensor based on un-doped and Cu-doped ZnO thin films," *Sensors and Actuators B: Chemical*, vol. 183, pp. 459-466, 2013. https://doi.org/10.1016/j.snb.2013.04.035

[31] V. Talwar, O. Singh, R. C. Singh, "ZnO/WO3 heterojunction based highly sensitive and selective ammonia sensor," *Sensors and Actuators B: Chemical*, vol. 191, pp. 276-282, 2014. https://doi.org/10.1016/j.snb.2013.09.102

[32] C. A. Skjøth, C. Geels, "The effect of climate change on European ammonia emissions and distribution," *Atmospheric Chemistry and Physics*, vol. 13, no. 1, pp. 117-128, 2013. https://doi.org/10.5194/acp-13-117-2013

[33] M. A. Sutton, J. W. Erisman, F. Dentener, D. Möller, "Ammonia in the environment: From ancient history to a 21st century challenge," *Environmental Pollution*, vol. 156, no. 3, pp. 583–604, 2008. https://doi.org/10.1016/j.envpol.2008.09.013

[34] S. S. Mali, C. K. Hong, "Porous hierarchical SnO2 structures as efficient electron transporting layers for stable perovskite solar cells," *Materials Today Chemistry*, vol. 17, p. 100336, 2020. https://doi.org/10.1016/j.mtchem.2020.100336

[35] A. K. Singh, R. Kumar, "Recent advances in TiO2-based solar-driven photocatalytic degradation of organic pollutants," *Journal of Environmental Chemical Engineering*, vol. 8, no. 4, p. 104012, 2020. https://doi.org/10.1016/j.jece.2020.104012

[36] R. Kumar, G. Agarwal, "Tailoring the electrical and optical properties of ZnO thin films by noble metal doping for sensor applications," *Materials Science in Semiconductor Processing*, vol. 134, p. 106042, 2021. https://doi.org/10.1016/j.mssp.2021.106042

[37] S. D. Shinde, A. V. Moholkar, "Synthesis, characterization and volatile organic compound sensing properties of sprayed SnO2 thin films," *Journal of Alloys and Compounds*, vol. 895, p. 162673, 2022. https://doi.org/10.1016/j.jallcom.2021.162673

[38] H. Qiao, L. Huang, "Enhanced photocatalytic efficiency of g-C3N4/TiO2 heterojunction for degradation of dyes under visible light," *Applied Surface Science*, vol. 571, p. 151319, 2022. https://doi.org/10.1016/j.apsusc.2021.151319

[39] D. K. Bandgar, S. T. Navale, "Flexible polyaniline/metal oxide hybrid nanocomposite films for high performance room temperature gas sensors," *Sensors and Actuators B: Chemical*, vol. 368, p. 132123, 2023. https://doi.org/10.1016/j.snb.2022.132123